

# Supplementary Information: An Autonomous Design Algorithm to Experimentally Realize Three Dimensionally Isotropic Auxetic Network Structures Without Compromising Density

Meng Shen<sup>1\*†</sup>, Marcos A. Reyes-Martinez<sup>2†</sup>,  
Louise Ahure Powell<sup>2</sup>, Mark A. Iadicola<sup>2</sup>, Abhishek Sharma<sup>1</sup>,  
Fabian Byléhn<sup>1</sup>, Nidhi Pashine<sup>3</sup>, Edwin P. Chan<sup>2</sup>,  
Christopher L. Soles<sup>2</sup>, Heinrich M. Jaeger<sup>3</sup>, Juan J. de Pablo<sup>1\*</sup>

<sup>1\*</sup>Pritzker School of Molecular Engineering, the University of Chicago,  
Chicago, 60637, IL, USA.

<sup>2</sup>Materials Science and Engineering Division, National Institute of  
Standards and Technology, Gaithersburg, 20899, MD, USA.

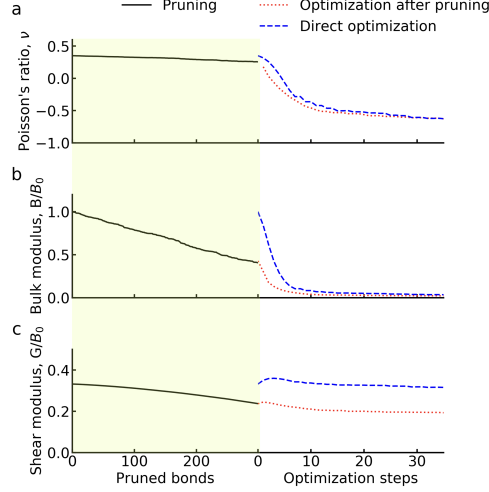
<sup>3</sup>Department of Physics, The James Franck and Enrico Fermi  
Institutes,, the University of Chicago, Chicago, 60637, IL, USA.

\*Corresponding author(s). E-mail(s): [depablo@uchicago.edu](mailto:depablo@uchicago.edu);

<sup>†</sup>These authors contributed equally to this work.

## Supplementary Note 1. Comparing local bond pruning method and global node optimization

Supplementary Figure 1 compares bond pruning method and global node optimization method on a initial network of coordination number  $Z = 7.2$ . The ratio of angle-bending resistance to bond-stretching resistance,  $k_\theta/k_b = 0.004$ , is an example of  $k_\theta \ll k_b$ . In the local bond-pruning method, in every iteration, every bond  $i$  is tentatively removed to measure  $\Delta G_i$ , and the bond leading to min  $\Delta G_i$  is permanently removed



**Supplementary Figure 1.** The changes in a) Poisson's ratio, b) bulk modulus,  $B$ , and c) shear modulus,  $G$ , of networks during local bond pruning and global node position optimization. The black solid curves in the left panel show the results for local bond pruning of an initial network of coordination number  $Z = 7.2$ . The red dotted curves in the right panel show the results for global node optimization of the pruned network whose coordination number is reduced to  $Z = 6.1$ . The blue dashed curves in the right panel show the results for direct global node optimization of an initial network of  $Z = 7.2$  directly from packing. The moduli are normalized by the bulk modulus of the original (unpruned) network,  $B_0$ .

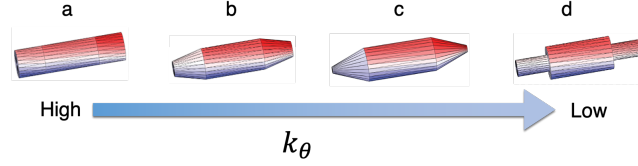
at the end of each iteration. In the global node optimization method, the position of the nodes are slightly adjusted iteratively to increase the ratio of the shear to bulk moduli,  $G/B$ , at each iteration.

The left panel of Supplementary Figure 1a shows that the reduction of  $\nu$  achieved by local bond-pruning is negligible even after 300 pruning steps. The left panel of Supplementary Figures 1b,c show that the reduction in shear modulus is on the same order of magnitude as the reduction in bulk modulus by local bond pruning, consistent with only a slight reduction in  $\nu$ . The inevitable reduction of  $G$  in the bond-pruning method restricts the further decrease of  $\nu$ , since  $\nu$  decreases with  $\frac{G}{B}$ .

After 300 iterations of local bond-pruning, the coordination number of the network is reduced from  $Z = 7.2$  to  $Z = 6.1$ . Global node optimization method is then applied to the pruned network with  $Z = 6.1$ . The red dotted curve in the right panel of Supplementary Figure 1a shows that global node optimization successfully brings  $\nu$  down below -0.5 after only about 25 iterations. Furthermore, we directly apply global node optimization method on the initial network with  $Z = 7.2$ . Interestingly, without any local bond pruning, the corresponding Poisson's ratio,  $\nu$ , of a network of  $Z = 7.2$ , is also reduced below -0.5 after only about 25 iterations (dashed curve in Supplementary Figure 1a), corroborating the effectiveness of global node optimization. The right panel of Supplementary Figures 1b,c show that global node optimization is not only effective

in reducing  $B$  for both networks but also effective in maintaining the shear modulus,  $G$ , indicating a more independent control of  $B$  and  $G$  than the bond pruning methods. Our results demonstrate that global node optimization is efficient in designing auxetic networks, without changing the coordination number.

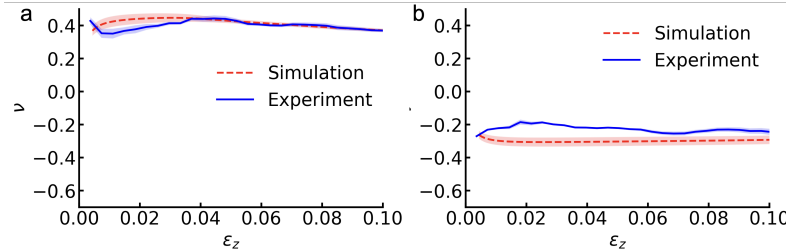
## Supplementary Note 2. Shapes of the bonds explored to transfer the computational design to 3D printing



**Supplementary Figure 2.** Bond-end considerations to reduce angle bending stiffness. The  $k_\theta/k_b$  values are expected to reduce from shape a to shape d.

Supplementary Figures 2a-d show different shapes of the bonds we tried. Theoretically, thinner soft materials close to the bond ends are desirable to satisfy the condition of  $k_\theta \ll k_b$ . In practice, thin bond ends are vulnerable to the cleaning process after supported 3D printing. Therefore, we choose the bond shape in Supplementary Figure 2b to measure the mechanical responses.

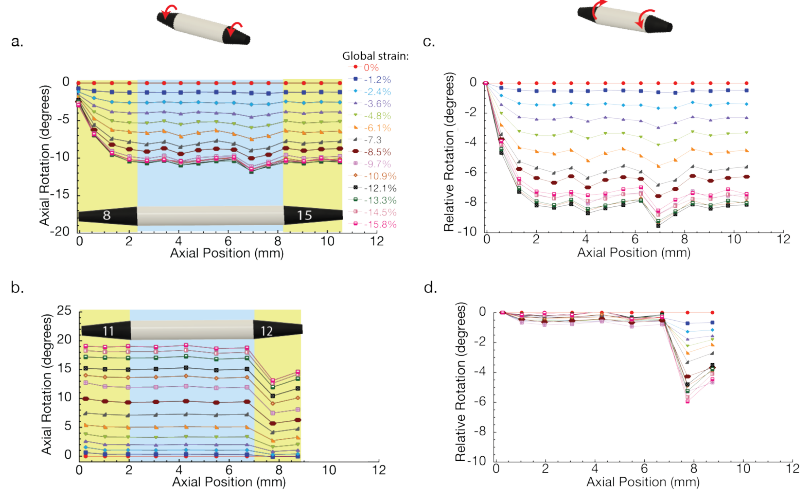
## Supplementary Note 3. Poisson's ratio as a function of strain



**Supplementary Figure 3.** Poisson's ratio as a function of strain of uniaxial compression from simulation (red dashed curves) and experimental validations (blue solid curves) for a) non-optimized initial network of coordination number  $Z = 6.1$  and b) optimized network of  $Z = 6.1$  at iter25.

Supplementary Figure 3 shows the Poisson's ratio as a function of strain from the measurements of both experimental and simulation networks of the coordination number  $Z = 6.1$ . For the network without global node optimization (Supplementary Figure 3a), in both simulation and experimental measurements, the Poisson's ratio is close to 0.4. For the network with global node optimization (Supplementary Figure 3b), in both simulation and experimental measurements, the Poisson's ratio is below -0.2 at small strains. The Poisson's ratio directly measured in both simulations and experiments here remain negative at least to a compression strain of 0.1. In experiments, the Poisson's ratio increases with the strain, but remains below -0.1 for a compression strain of 10%.

## Supplementary Note 4. Digital Image Correlation of Select Bonds



**Supplementary Figure 4.** Digital Image Correlation (DIC) analysis of representative bonds and nodes as a function of axial position. a) Absolute axial rotation as a function of axial position along the 8-15 bond. b) Relative axial rotation along axial position with respect to node 8. c) Absolute axial rotation as a function of axial position along the 11-12 bond. d) Relative axial rotation with respect to node 11 as a function of axial position.

We perform Digital Image Correlation (DIC) analysis on two representative surface bonds with their respective nodes. This DIC analysis was compared on the bond between nodes 8 and 15 (Supplementary Figure 4a), as an example of where the simulated trajectory of nodes displayed good agreement with experiment, with the bond between nodes 11 and 12 (4b), as an example of where the simulated trajectory

of the nodes deviate from experiment at high strains. Supplementary Figure 4a shows that as the global compressive strain increases, the entire soft and stiff portions of bond rotate in concert about the bond axis with the exception of node 8, which rotates less than the rest of the bond. The increase in the axial rotation slows down after 9.7 % global strain due to a minor contact from another bond (See **Supplementary Video 2**). As the uniaxial compression increases, the relative rotation (Supplementary Figure 4c) shows an angle difference of less than 10 degrees between node 8 and the rest of the bond, indicating a minor development of twist with respect to node 8. For the case of the bond between nodes 11-12, Supplementary Figure 4d shows that the entire bond (both stiff and soft portions) rotate almost concomitantly, with comparatively smaller rotation observed on node 12. As the compression increases, the rate of increase in axial rotation fluctuates after 8.5 % strain due to member contact with a another bond connected to node 12 (See **Supplementary Video 3**). This contact causes directional shifts in the twist angle. As the compressive strain increases, a twist of less than 6 degrees develops in node 12 compared to the rest of the bond.

## Supplementary Note 5. Importance of Torsional Constraints in Simulations

The Hamiltonian for the optimization simulations is written as:

$$H = U = \frac{1}{2} \sum_i k_{bi} \frac{(l_{bi} - l_{b0i})^2}{l_{b0i}^2} + \frac{1}{2} \sum_m k'_{\theta m} (\theta_m - \theta_{0m})^2 \quad (1)$$

where  $U$  is the potential energy,  $k_b$  and  $k'_\theta$  are the bond stretching resistance and angle bending resistance, respectively.  $k'_\theta = \frac{2k_\theta}{N_c - 1}$ , where  $k_\theta$  is the total angle bending stiffness per bond with respect to each node, and  $N_c$  is the coordination number.

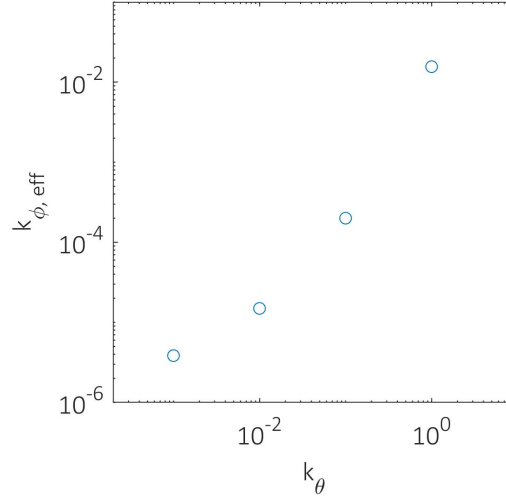
While the above model only incorporates bond stretching and angle bending resistance, another common mechanical constraint in such systems is the resistance to bond torsion. In this section we demonstrate that in these highly coordinated networks, including torsional constraints are not necessary as the bond stretching and angular bending constraints also effectively resist bond torsion. This analysis complements the experimental results using DIC. To study this we evaluate an effective torsional constant imparted by these constraints onto the network. We evaluated this by compressing a mechanical network along one axis and then minimizing the mechanical energy in LAMMPS as used in other parts of the work. Then we equate the residual energy  $U_{res}$  in the mechanical constraints with a hypothetical torsional energy:

$$U_{res} = \sum_{bonds} \frac{1}{2} k_{\phi,eff} (\Delta\phi)^2 \quad (2)$$

resulting from the torsion of the bonds  $\Delta\phi$ . We calculate the torsion  $\Delta\phi$  as the average of signed dihedral angles associated with the bond. Assuming all bonds have the same torsional constant, we can rearrange the expression for  $k_{\phi,eff}$  as:

$$k_{\phi,eff} = 2 \times U_{res} / \sum_{bonds} (\Delta\phi)^2 \quad (3)$$

We deformed configurations with 504 nodes with  $Z \approx 6.1$  as used elsewhere in the paper. We compressed the box along one axis by  $\approx 0.1\%$ , which resulted in a maximum torsion below  $1^\circ$  in all cases. We kept  $k_b = 1$  while  $k_\theta$  was varied. The results are shown in Supplementary Figure 5. Our results demonstrate that effective torsional constant rises dramatically in response to the increase in the strength of the angular constraint. This indicates that torsional constraints may not be necessary to capture the mechanical response in highly coordinated networks with sufficiently strong bond and angular constraints.



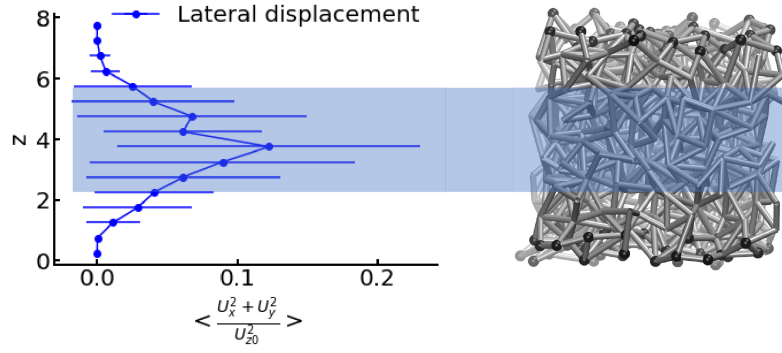
**Supplementary Figure 5.** Variation of  $k_{\phi,eff}$  as a function of  $k_\theta$

## Supplementary Note 6. Quantifying elastic isotropy in simulations

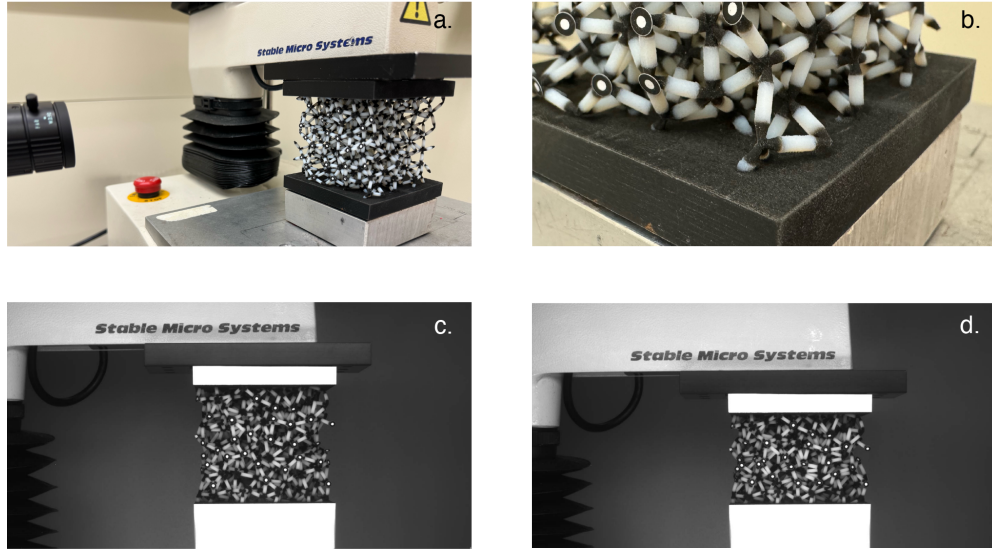
For isotropy, the stiffness matrix should have the form:  $C_{11} = C_{22} = C_{33}$ ,  $C_{12} = C_{13} = C_{23}$ ,  $C_{44} = C_{55} = C_{66}$ , while the rest of the constants are equal to 0. An example for the elastic stiffness matrix of a simulated node-optimized network shows that it can be considered isotropic within approximately  $\pm 3$  GPa.

$$C = \begin{pmatrix} 30.06 & -10.34 & -11.51 & 0.93 & -0.16 & -0.50 \\ 0 & 29.71 & -11.31 & -3.65 & 0.16 & 0.19 \\ 0 & 0 & 31.07 & 2.77 & 0.31 & -0.06 \\ 0 & 0 & 0 & 22.34 & 0.65 & 0.89 \\ 0 & 0 & 0 & 0 & 25.39 & -2.04 \\ 0 & 0 & 0 & 0 & 0 & 24.30 \end{pmatrix} \text{ GPa}$$

## Supplementary Note 7. Experimental realization



**Supplementary Figure 6.** Lateral displacement of node-optimized mechanical metamaterial with top and bottom surface node constraints. Black nodes indicate laterally-constrained surface nodes.



**Supplementary Figure 7.** Experimental setup for measuring mechanical properties of physical realizations of node-optimized mechanical metamaterials. a) Disordered network metamaterial in compression frame. b) Surface nodes can be seen embedded in added flat plate. c) Photograph of network sample at zero strain. d) Photograph of network sample during compression.